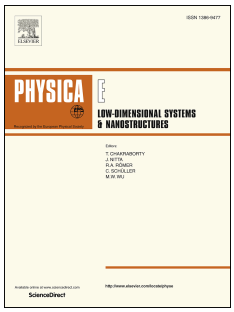

Electronic structure and carrier mobilities of twisted graphene helix

Rajesh Thakur, P.K. Ahluwalia, Ashok Kumar, Brij Mohan, Raman Sharma

PII: S1386-9477(19)31865-X

DOI: https://doi.org/10.1016/j.physe.2020.114280

Reference: PHYSE 114280

To appear in: *Physica E: Low-dimensional Systems and Nanostructures*

Received Date: 11 December 2019

Revised Date: 19 May 2020

Accepted Date: 4 June 2020

Please cite this article as: R. Thakur, P.K. Ahluwalia, A. Kumar, B. Mohan, R. Sharma, Electronic structure and carrier mobilities of twisted graphene helix, *Physica E: Low-dimensional Systems and Nanostructures* (2020), doi: https://doi.org/10.1016/j.physe.2020.114280.

Electronic Structure and Carrier Mobilities of Twisted Graphene Helix

Rajesh Thakur*[$], P. K. Ahluwalia[$], Ashok Kumar[&], Brij Mohan[#], and Raman Sharma[$]

[$]*Department of Physics, Himachal Pradesh University, Summer Hill, Shimla 171005 Himachal Pradesh (INDIA)*

[&]*Department of Physics, School of Basic and Applied Sciences, Central University of Punjab, Bathinda, 151001 Punjab (INDIA)*

[#]*Department of Physics, Govt. Degree College Sanjauli, Shimla-171006, Himachal Pradesh (INDIA)*

(April 2020)

*Corresponding author: Email: rajeshhputhakur@gmail.com

Abstract

Density functional theory based calculations have been carried out to investigate the effect of twisting on electronic band structures and carrier mobilities of three prototypes of armchair graphene nanoribbons (AGNRs) within the fixed boundary conditions. It is found that twisting causes a modification in the bandgap values and the overall shape of band structures. The values of longitudinal acoustic deformation potential (DP) are found to be higher than the torsional acoustic DP values. The torsional strain is also found to have a profound effect on effective mass and mobilities of given AGNRs. The hole mobility of hydrogen passivated N=8 AGNRs is found to be comparable with the carrier mobility of intrinsic graphene. The electron mobility of N=8 AGNRs can be further increased with fluorine passivation. The width, passivation, and extent of twisting together determine n-type or p-type behavior of AGNRs. Fluorine passivated AGNRs are predicted to be potential candidates for mechanical and high-frequency switching. Our results suggest that twisting of AGNRs can be an effective mean for tuning their band structure and carrier mobility for applications in high-speed switching devices.

1. Introduction

Graphene, the most stable single-layer two-dimensional hexagonal structure of carbon atoms, exhibits unique electronic band structure. However, lack of bandgap limits its application in electronic devices. Various ways to introduce a bandgap in graphene have been suggested in the literature [1–3]. One of these ways is the synthesis of graphene nanoribbons (GNRs) [4,5], which not only creates a bandgap but also offers some novel mechanical properties [6–8]. These GNRs can be utilized as nano-switches [9], negative differential resistance materials [10], magnetic resistance materials [11], spin filters [12] and nanosensors [13,14]. Depending on the edge direction, these GNRs can be categorized into zigzag graphene nanoribbons (ZGNRs) with metallic properties and armchair graphene nanoribbons (AGNRs) with semiconductor and semi-metallic properties [7,15,16].

The electronic properties of GNRs can be modified by twisting [8]. Although, twisting does not change the bandgap of ZGNRs significantly [9], but twisted AGNRs (width <1 nm) show a substantial change in the electronic structure [8]. Twisted GNRs form chiral helical structures which can be fabricated by a range of methods [6,17,18]. Twisted GNRs can also function as a field-effect transistor or a device with non-linear current-voltage characteristics [10].

Bandgap of AGNRs has been found to be periodically oscillating as a function of uniaxial strain[19]. Also, a shift in the band energy surfaces in the Brillouin zone can also be introduced by twisting as found in the case of carbon nanotubes [20]. Therefore, it is interesting to investigate the edge passivated AGNRs beyond uniaxial strain deformation to torsional deformation.

In this paper, the effect of twisting and passivation on the electronic band structure of AGNRs has been studied within the fixed boundary condition making translational symmetry

tractable only for a few discrete twist angles values (θ) in bipartite lattice [17,21–23]. The bandgaps of AGNRs depend on the number of dimers (N) along zigzag direction [24] which can be further grouped into three families, namely, (i) $N = 3n - 1$ family exhibiting smallest bandgaps, (ii) the $N = 3n$ family exhibiting medium bandgaps, and (iii) $N = 3n + 1$ family exhibiting largest bandgaps, where n is a positive integer [8]. One case of each of the classes for Hydrogen(H)-terminated AGNRs i.e. HAGNRs and Fluorine (F)-terminated AGNRs i.e. FAGNRs [25–27] has been carried out for N=6, 7 and 8.

2. Computational Details

All the spin-polarized density functional theory calculations in this work are performed using the SIESTA [28] package. Norm conserving Troullier-Martins pseudopotential in fully separable Kleinman and Bylander form has been used to treat the electron-ion interactions [29]. The exchange and correlation energies have been treated within GGA-PBE functional [30]. Although the bandgap of GNRs when calculated with GGA-PBE functional is underestimated as compared to measured bandgap [31,32], the choice of this functional is guided by the fact that it produces the other properties of AGNRs like effective mass [33,34] or work function [35] in good agreement with the experimental studies [31,36]. Also this functional has been found to produce carrier's effective mass and mobility with reasonable accuracy in case of Phosphorene nanoribbons (PNRs) [37].

The Kohn-Sham orbitals were expanded as a linear combination of numerical pseudo-atomic orbitals (PAO) using a split-valence double-zeta polarized (DZP) basis sets with confinement energy of 0.01 Ry. The convergence tolerance for total energy is chosen to be $10^{-5} eV$ between two consecutive steps. Minimization of energy was carried out using standard conjugate-gradient (CG) technique. Converged values of sampling for the k-mesh

grid $\sim 10^{-2}\text{Å}^{-1}$ have been used according to Monkhorst-Pack scheme [38] to sample the Brillouin zone (See supplementary information).

Structures chosen with a fixed lattice constant were relaxed until force on each atom was less than $10^{-2} eV\text{Å}^{-1}$. Mesh cut-off energy used to expand the Kohn-Sham orbitals was 800Ry for untwisted AGNRs and the converged values ranged between 1300Ry to 1450Ry for twisted AGNRs. The distance between the two periodic ribbon images taken perpendicular to the helix axis (X and Y-axis) is 13.82 Å, 12.63 Å, and 11.4 Å for N=6, 7 and 8 respectively. A unit cell of dimension $20\text{Å} \times 20\text{Å}$ along X-Y direction was taken which ensures more than~11 Å distance between the periodic images to prevent the superficial interactions.

3. Results and Discussion

We have classified different helical conformations presented here by three parameters shown in Figure 1: The L_M is the lattice constant in Z-direction, W is the width of AGNR from one carbon edge atom to another carbon edge atom on the opposite edge along the zigzag direction. The width (W) corresponds to the number of dimers (N) along the zigzag direction is labeled from 1 to N as given in Table 1. The subscript $\boldsymbol{M}$ of lattice constant $\boldsymbol{L_M}$ is the number of times unit-cell get repeated or multiplied to have required twisted supercell structure. In our previous study [39] we have explained the method to determine the $\boldsymbol{L_M}$.

The lattice parameters of the studied nanoribbons (HAGNRs and FAGNRs) are given in Table 1. The mechanics of the transition of planar AGNR to helical shaped conformation is shown in Figure 1(a-b). Increase in torsional angle decreases the unit cell size $\boldsymbol{L_M}$ and increases the torsional strain as indicated in Figure 1(b-c). We have also modeled the study

on a few discrete torsional angles compatible with translation symmetry along Z-direction for HAGNRs and FAGNRs.

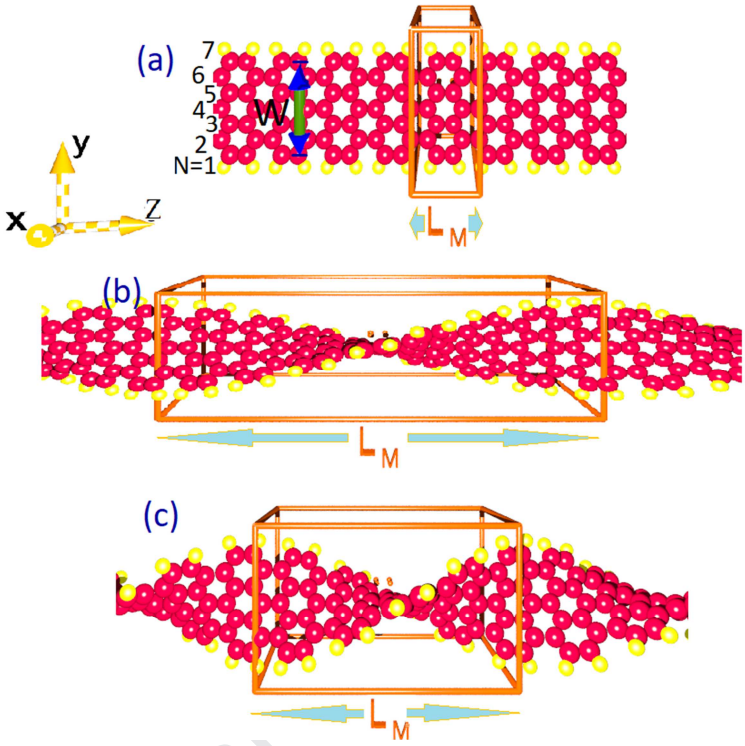

Figure 1: Schematic description of mechanics of twisting of AGNRs periodic in Z direction. (a) Planar untwisted N=7 AGNR with a minimum lattice constant L_M (torsional angle θ=zero). Torsional strain morphs planar AGNR into (b) helical shaped infinite long helix with the increased value of lattice constant that eventually shrinks to (c) a helix with a much smaller lattice constant on further twisting.

3.1. Electronic properties

The electromechanical response of twisted helixes has been investigated by studying the effect of effective strain on the three most important physical quantities: bandgap, effective mass and carrier mobility. The effective strain, $\boldsymbol{\varepsilon^{eff}}$, associated with the twist angle (θ) is given by $\varepsilon^{eff} = 1/2(\theta^2 \Sigma_n^2)$, where Σ_n is the distance of n^{th}dimer from the AGNR axis [40]. The calculations reveal that among the untwisted passivated AGNRs, H- and F-AGNR with N=6 have the highest bandgap of 1.14eV and 1.41eV, respectively, which increases to 2.01 eV for HAGNRs under extreme torsional strain. However, in the case of FAGNRs (for N=6), bandgap does not vary much (See *Figure 2*).

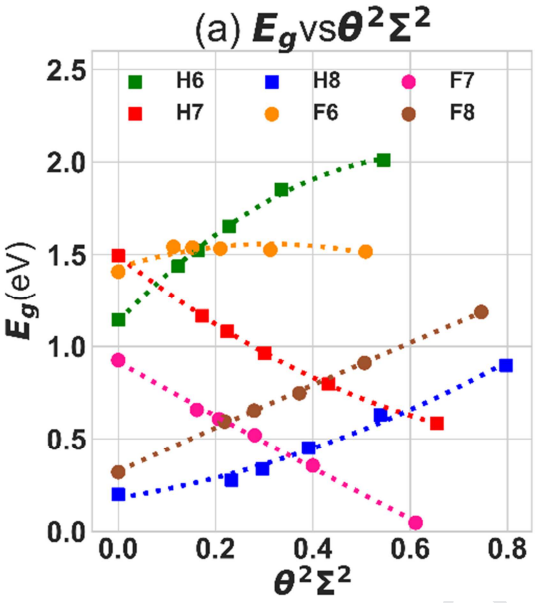

Figure 2: Bandgap as a function of effective strain for different width nanoribbons.

Because of the sub-lattice symmetry, direct bandgap at the high symmetry Γ-point for untwisted H-AGNRs (N=6) gets shifted to high symmetry point $\pm K$ under torsional strain (Figure 3) except for most twisted case (torsional angle=0.207 rad) where the bandgap of 2.01eV transits to indirect bandgap (Figure 3f). However, the untwisted F-AGNRs (N=6) exhibits a direct bandgap of 1.41eV at Γ(Figure S1a) which turns to indirect bandgap promptly when subjected to mild twist (Figure S1 (b to f)).

Unlike a direct-to- indirect bandgap transition at the critical torsional strain in H- and F-AGNRs (N=6) helixes, the H- and F-AGNRs (N=8) do not show any such transition, and the bandgap remains direct at high symmetry point Γ for helixes of all torsional angles (Figure 4(b to f) and Figure S2(b to f)). Similar to helixes of N=6, a shift of direct bandgap from Γ to $\pm K$ has been found for helixes of N=7 when subjected to twist. However, in this case, the bandgap remains direct at the high symmetry point $\pm K$ for all twisted topologies (Figure 5(b to f) and Figure S3 (b to f)). In the effective strain space, the trend of bandgap response to torsional strain suggested a monotonous increasing behavior for N=6 and 8 HAGNRs (i.e. N=3 and N=3n+2; where n is positive integer), categorizing them into one family. Another

important observation can be made from the spin-degenerate band structure of all topologies.

No net magnetic moment has been observed in any considered case.

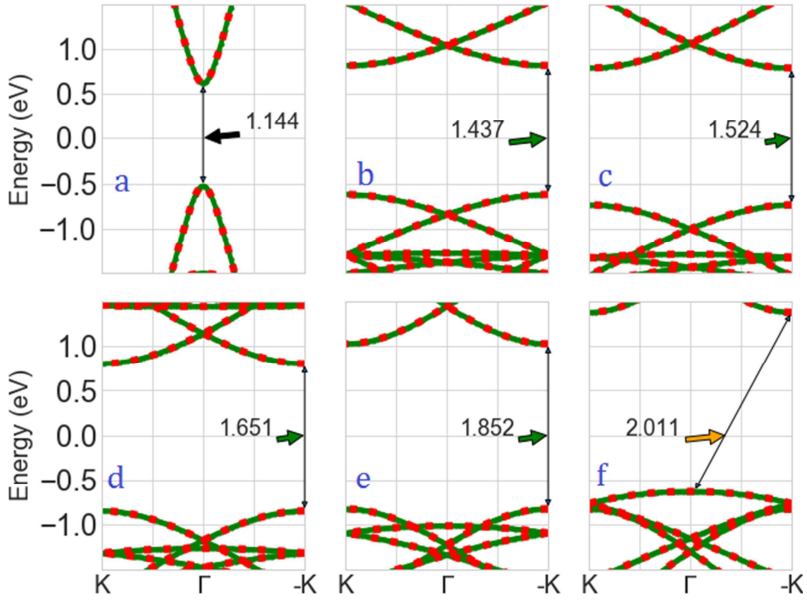

Figure 3: ***Calculated spin-polarized band structure of (a) Untwisted 6-HAGNR and twisted 6-HAGNRs with torsional angle values (b) 0.097rad (c) 0.112rad (d) 0.132rad (e) 0.161rad (f) 0.207rad . The order of the magnitude of torsional strain is a=0< b < c < d < e < f.***

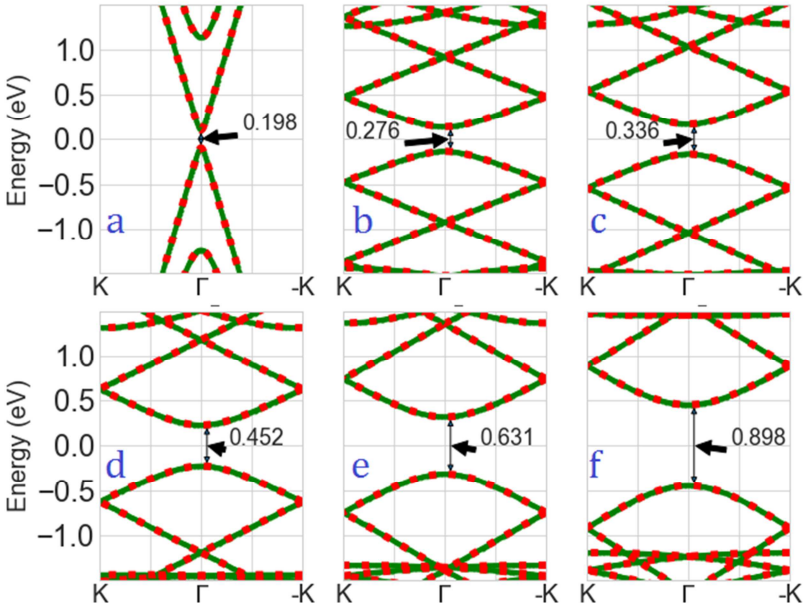

Figure 4: ***Calculated spin-polarized band structure of (a) Untwisted 8-HAGNR and twisted 8-HAGNRs with torsional angle value (b) 0.086rad (c) 0.097rad (d) 0.112rad (e) 0.132rad (f) 0.162rad. The order of the magnitude of torsional strain is a=0< b < c < d < e < f.***

For N=7 helixes (H- and F-AGNRs), the behavior of bandgap as a function of effective torsional strain is monotonous and linear but with a negative slope Figure 2. This kind of behavior categorizes the $\boldsymbol{N}$=7AGNR (i.e. $N=3n+1$; n is a positive integer) into a different family. In comparison to the bandgap values of all N=7HAGNR helixes (red square in Figure 2), it is obvious that F passivation of N=7 AGNRs helixes reduces the bandgap values (pink circle in Figure 2). In the case of N=8 F-AGNR helixes, bandgap values (brown circles in Figure 2) are higher than the N=8 HAGNR helixes values (blue squares in Figure 2).

The anomalous behavior of N=6 AGNRs helixes can be understood through our previous study [39] in which we calculated net charge accumulation on H and F atoms using Hirshfeld method [41]. The net charges accumulation on H and F atoms is $\boldsymbol{\Delta Q}$= 0.022e and $\boldsymbol{\Delta Q}$ = -0.030e, respectively. We found that the net charge accumulation does not vary either on twisting or by changing the dimer number $\boldsymbol{N}$. This means that the F atoms pull more electrons from the bonding C atoms, thus, the depletion of electron charge density from the carbon hexagons of N=6 F-AGNRs is more than any other HAGNRs and N=7 and 8 FAGNRs.

Furthermore, because of the reduction of about ~0.5eV in the bandgap values of F-AGNRs (N=7) compared to H-AGNRs (N=7) and twisting to extreme point the Dirac cone appears at $\pm\boldsymbol{K}$ point (Figure S3). This linear dispersion allows the electrons to flow ballistically through a '*strongly twisted'* N=7 FAGNRs.

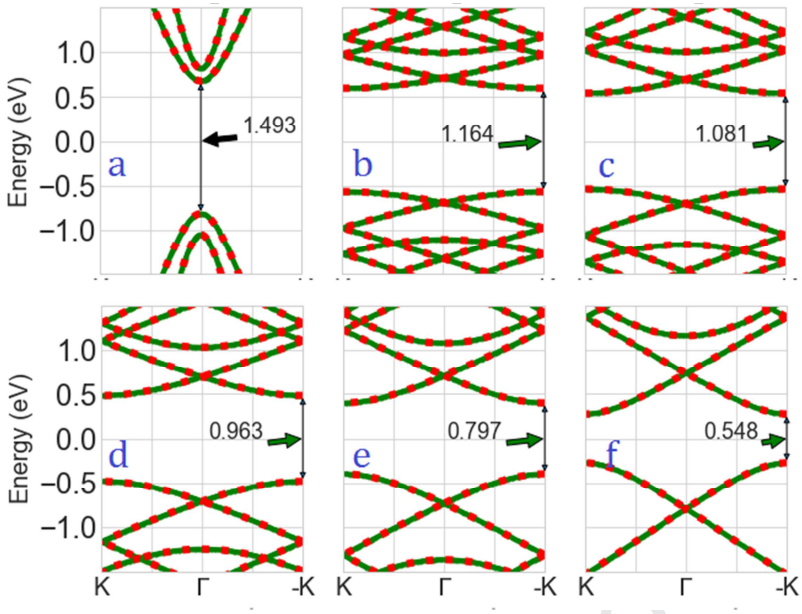

Figure 5:*Calculated spin-polarized band structure of (a) Untwisted 7-HAGNR and twisted 7-HAGNRs with torsional angle value (b) 0.091rad (c) 0.104rad (d) 0.121rad (e) 0.146rad (f) 0.182rad. The order of the magnitude of torsional strain is a =0 < b < c < d < e < f.*

3.2. Effective Mass and Mobility

We calculated the carriers transport by applying deformation potential (DP) theory [42] and effective mass approximation. In an earlier study of carbon nanotubes, it has been observed that along with the stretching and breathing modes the twisting mode also contributes to the electron-phonon scattering [20]. Deformation in GNRs can be made by (i) the longitudinal uniaxial strain ε_{zz}, which represents the stretching mode, (ii) the torsional strain $\varepsilon_{z\theta}$, which represents the twisting mode and (iii) the lateral strain ε_{yy}, which represents the breathing mode. The band edge can be expressed as $E(\varepsilon_{ij}) = E_0 - E_{1L}\varepsilon_{zz} - E_{1T}\varepsilon_{z\theta} - E_{1B}\varepsilon_{yy}$ for one dimensional AGNRs [42], where E_{1L}, E_{1T} and E_{1B} represent the deformation potential (DP) value for three different modes. The longitudinal acoustic DP $E_{1L} = \delta(E_{edge} - eV_{Vaccum})/\delta\varepsilon_{zz}$, where $\delta(E_{edge} - eV_{Vaccum})$ is the shift of conduction band maxima (CBM) or valance band minima (VBM) with respect to the energy of vacuum level, (eV_{Vaccum}) is calculated for the considered AGNRs.

Table1: **Structural parameters, Bandgap (E_g), Effective masses at VBM ($|m_h^*|/m_e$) and CBM ($|m_e^*|/m_e$) and predicted carrier mobility for hole (μ_{1D}^h) and electron (μ_{1D}^e). Results of previous studies theoretical** [24]$^{@}$**,** [43]$^{\#}$**,** [33]$^{*\#}$**,** [44]***and** [45]$^{\$}$**; experimental** [36]$^{\&}$**,** [33]**

	L_M Å	θ radÅ^{-1}	E_g eV	$\lvert m_h^*\rvert/m_e$	m_e^*/m_e	μ_{1D}^h $cm^2V^{-1}s^{-1}$	μ_{1D}^e $cm^2V^{-1}s^{-1}$	W Å
6-HAGNR	$4.325_{1.0}$	Zero	1.144	0.127, 0.12*	0.125, 0.12*	$2.92x10^2$	$4.30x10^4$	6.15, 6.15$^{\#}$, 6.19$^{\$}$
	$32.439_{7.5}$	0.097	1.437	0.133	0.133	$2.74x10^2$	$3.93x10^4$	6.133
	$28.114_{6.5}$	0.112	1.524	0.143	0.138	$2.45x10^2$	$3.69x10^4$	6.123
	$23.789_{5.5}$	0.132	1.651	0.166	0.159	$1.96x10^2$	$3.0x10^4$	6.110
	$19.464_{4.5}$	0.161	1.852	0.179	0.173	$1.75x10^2$	$2.64x10^4$	6.085
	$15.139_{3.5}$	0.207	2.011	0.303	0.237	$7.91x10^1$	1.65x104	6.030
7-HAGNR	$4.32_{1.0}$, 4.2$^{\&}$	Zero	1.493	0.31, 0.33$^{*\#}$, 0.41**	0.35,0.41$^{*\#}$, 0.40**	$2.0x10^3$	$8.92x10^1$	7.37, 7.31$^{\#}$,7.34$^{\$}$
	$34.525_{8.0}$	0.091	1.164	0.255	0.232	$2.53x10^3$	$1.6x10^2$	7.324
	$30.209_{7.0}$	0.104	1.081	0.2193	0.219	$3.17x10^3$	$1.74x10^2$	7.307
	$25.894_{6.0}$	0.121	0.963	0.2042	0.216	$3.53x10^3$	$1.78x10^2$	7.274
	$21.578_{5.0}$	0.146	0.797	0.1762	0.155	$4.40x10^3$	$2.9\ x10^2$	7.224
	$17.262_{4.0}$	0.182	0.548	0.1332	0.151	$6.70x10^3$	$3.05x10^2$	7.131
8-HAGNR	$4.31_{1.0}$, 4.35$^{@}$	Zero	0.198	0.031,0.04*	0.031,0.04*	$4.0x10^4$	$2.42x10^3$	8.63, 8.67$^{\#}$, 8.66$^{\$}$
	$36.720_{8.5}$	0.086	0.276	0.037	0.037	$3.65x10^4$	$2.17x10^3$	8.574
	$32.325_{7.5}$	0.097	0.336	0.046	0.046	$2.64x10^4$	$1.57x10^3$	8.564
	$28.015_{6.5}$	0.112	0.452	0.061	0.064	$1.72x10^4$	$9.65x10^2$	8.535
	$23.705_{5.5}$	0.132	0.631	0.089	0.097	$9.82x10^3$	$5.14x10^2$	8.493
	$19.395_{4.5}$	0.162	0.898	0.139	0.148	$5.04x10^3$	$2.74x10^2$	8.420
6-FAGNR	$4.443_{1.0}$	Zero	1.407	0.137	0.125	$4.17x10^2$	$9.50x10^3$	6.068
	$33.322_{7.5}$	0.094	1.543	0.781	0.260	$30.6x10^1$	$3.17x10^3$	6.059
	$28.879_{6.5}$	0.109	1.539	1.040	0.173	$2.0x10^1$	$5.85x10^3$	6.052
	$24.436_{5.5}$	0.128	1.533	1.017	0.161	$2.1x10^1$	$6.49x10^3$	6.046
	$19.993_{4.5}$	0.157	1.526	0.893	0.241	$2.5x10^2$	$3.55x10^3$	6.020
	$15.551_{3.5}$	0.202	1.517	0.837	0.299	$2.76x10^2$	$2.58x10^3$	5.967
7-FAGNR	$4.421_{1.0}$	Zero	0.926	0.179	0.176	$8.67x10^3$	$2.98x10^2$	7.263
	$35.368_{8.0}$	0.089	0.658	0.115	0.115	$1.67x10^4$	$5.63x10^2$	7.239
	$30.947_{7.0}$	0.101	0.608	0.101	0.101	$2.04x10^4$	$6.87x10^2$	7.222
	$26.526_{6.0}$	0.118	0.520	0.103	0.103	$1.99x10^4$	$6.69x10^2$	7.194
	$22.105_{5.0}$	0.142	0.355	0.074	0.074	$3.27x10^4$	$1.10x10^3$	7.141
	$17.684_{4.0}$	0.178	0.048	Massless	Massless	--	--	7.043

8-FHGNR	$4.411_{1.0}$	Zero	0.319	0.046	0.046	$1.82x10^3$	$4.15x10^5$	8.540
	$37.494_{8.5}$	0.084	0.595	0.080	0.076	$8.0x10^2$	$1.94x10^5$	8.510
	$33.083_{7.5}$	0.095	0.654	0.094	0.089	$6.27x10^2$	$1.51x10^5$	8.494
	$28.672_{6.5}$	0.110	0.748	0.110	0.110	$4.94x10^2$	$1.11\ x10^5$	8.469
	$24.261_{5.5}$	0.129	0.912	0.139	0.139	$3.47x10^2$	$7.77x10^4$	8.424
	$19.850_{4.5}$	0.158	1.186	0.188	0.208	$2.22x10^2$	$4.26x10^4$	8.351

The DP term for twisting mode has been obtained as $E_{1T} = \delta(E_{Edge} - eV_{Vaccum})/\delta\varepsilon^{eff}$ where E_{Edge} is the VBM for holes or the CBM for electrons. Within the elastic limits, the magnitude of DP describes the degree of interaction between electrons and phonons. Therefore, the small value of DP indicates a weak electron-phonon interaction, which results in high mobility of charge carriers**.** Accordingly, for 1D systems the carriers' mobility is $\mu_{1D} = \frac{ne\hbar^2 C_{1D}}{(2\pi k_B T)^{\frac{1}{2}}|m^*|^{\frac{3}{2}}E_1^2}$, where T=300K, and C_{1D} is the stretching modulus caused by uniaxial strain which has been calculated using the expression $C_{1D} = \frac{1}{L_0}\frac{d^2}{d\varepsilon^2}E_\varepsilon$ where E_ε is the strain energy of a unit cell [46]. In the case of the parabolic bands, the effective mass is calculated from band energy (E_{nk}) versus wave vector (k) curve by $m^{*-1} = \hbar^{-2}\frac{\partial^2 E_{nk}}{\partial k^2}$.

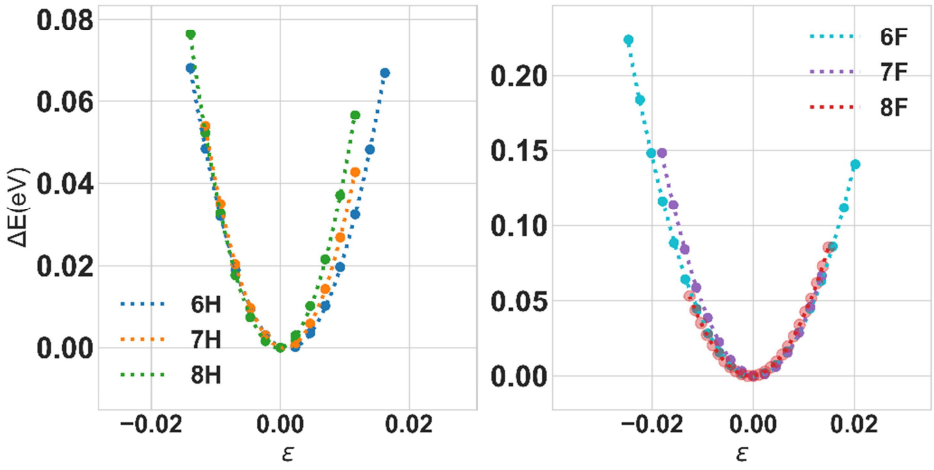

Figure 6: ***Energy−strain relationship in an armchair direction of (a) HAGNR and (b) FAGNR.***

The variation of difference in strain energy (ΔE) with the uni-axial strain (ε) applied along the armchair directions is shown in Figure 6. Based on these energy-strain curves we have calculated the line-stiffness coefficient C_{1D} given in Table 2 which comes out to be smaller than that in a previous study [44]. The values of C_{1D} of N=6, 7 and 8 HAGNRs are by about 12% smaller than those of their FAGNRs counterparts. The magnitude of calculated longitudinal acoustic DPs for electrons and holes carriers are given in Table 2. In earlier reported studies the value of E_{1L} varies significantly [44] and, [15] because of the different reference energy points taken in these studies. We followed the method described in ref. [15] for determining E_{1L}, the calculated values are in fair agreement with the earlier reported values as shown in Table 2.

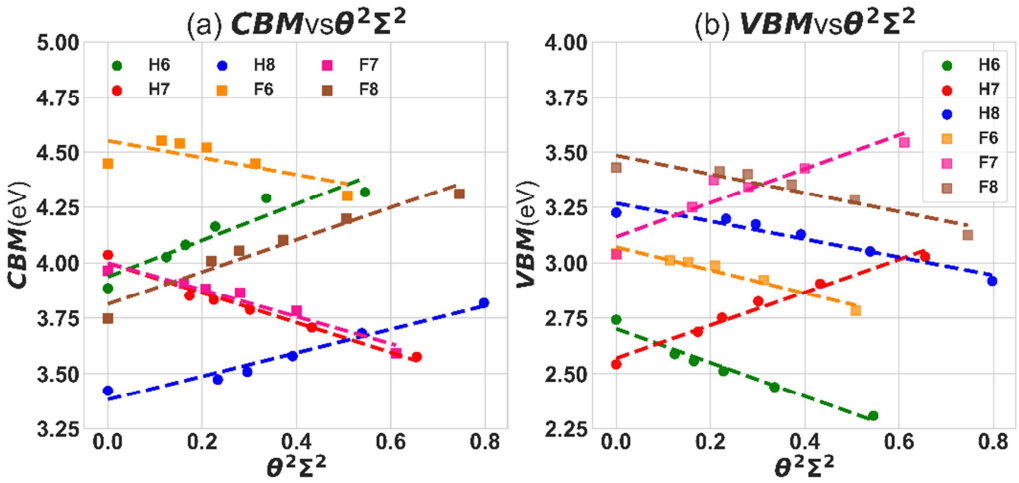

Figure 7: ***Shift of valance band minima (VBM) and conduction band maxima (CBM) under effective torsional strain for different cases. The dashed lines are the linear fitting.***

Figure 7 shows the shifts of band edges as a function of effective torsional strain along the armchair direction. The torsional DP (E_{1T}) is then calculated as $dE_{Edge}/d\varepsilon^{eff}$, equivalent to the slope of the fitting lines, where E_{Edge} is the energy of the conduction (valence) band edge. The E_{1T} values of H- and F-AGNRs are shown in Table 2. Except for N=6 FAGNRs helix, the standard deviation of all E_{1T} values is smaller than 1%. The lattice scattering is determined by the shifts in the band's energy resulting from dilations associated with acoustic waves [42]. The higher value of shift in the band energy occurred because of stretching mode, therefore, only the longitudinal DP value is taken for determining the mobilities. As we will see that the effective mass's response to twisting has a profound effect on mobilities.

Based on the obtained energy band spectrum and calculated values of E_{1L}, E_{1T}, *and* C_{1D} we determined the acoustic phonon-limited mobility at room temperature (300 K). As was already concluded, the scattering rate of carriers in AGNRs is dominated by the longitudinal acoustic mode, rather than by the twisted mode. However, the longitudinal acoustic DPs for an electron of N=6 HAGNR and N=8 FAGNR helixes are 0.30eV and -0.57eV, respectively, which are smaller than that of remaining considered helixes. This implies that the electron-phonon interaction is very small for N=6 HAGNR and N=8 FAGNR helixes which promotes very high mobility.

Table 2: The line stiffness (C_{1D}), the longitudinal DP (E_{1L}) and torsional DP (E_{1T}) of Hydrogen and Fluorine passivated AGNRs. [15][@] [44][#]

	C_{1D} $(10^{12}\ eV/m)$	E_{1L} of electron (eV)	E_{1T} of electron (eV)	E_{1L} of hole (eV)	E_{1T} of hole (eV)
6HAGNR	2.96, 3.96[#]	0.30, *0.84*[@]	-0.76	9.11	0.82
7HAGNR	3.32, 4.28[#]	8.59, *9.36*[@]	0.74	-2.01	-0.67
8HAGNR	3.34, 4.29[#]	9.79, *10.41*[@]	-0.40	-2.39	0.53
6FAGNR	3.22	1.74	-0.52	7.76	-0.39
7FAGNR	3.76	8.23	0.77	-1.51	-0.61
8FAGNR	3.78	-0.57	-0.43	8.53	0.73

Based on the obtained band structures, we calculated the effective mass of the charge carrier by parabolic fitting of bands near the band edges (Table 1). It is found that the values of carrier effective masses are small which means that the AGNRs have considerably high carrier mobility. The value of effective mass ($|m^*|/m_e$) is observed to be very sensitive to twisting. The response of electron and holes mobilities as a function of effective strain is shown in Figure 8. Our results show that the $|m^*|/m_e$ for electrons (holes) in untwisted 6, 7 and 8 HAGNRs are 0.13 (0.13), 0.34 (0.30) and 0.03 (0.03), respectively, which are in good agreement with the values reported by Fischetti et. al. [15]. The value of $\frac{|m^*|}{m_e}$ for electrons and holes in untwisted N=7 HAGNRs are also in good agreement with the values reported by Senkovskiy et. al. [34] and Sode et. al. [33]. Furthermore, it can be seen from Table 1 that the effect of F passivation on the effective mass of electron or hole for N= 7 and N=8 is small, however, a drastic change for N=6 is noticed. Our results also show the response of twisting for N=7 where the $|m_e^*|/m_e$ ($|m_h^*|/m_e$) decreases from 0.34 to 0.15 (0.29 to 0.13) for H-AGNRs and 0.18 to zero (0.18 to zero) for FAGNRs. However, opposite trend is observed for N=6 and 8 *i.e.* the $|m_e^*|/m_e$ ($|m_h^*|/m_e$) values increased as a response to twisting, as shown in Figure 8. Furthermore, it is clearly seen that even for the most mild twisting, the $|m_h^*|/m_e$

for N=6 FAGNRs helixes becomes bigger than the $|m_e^*|/m_e$. This indicates an n-type behaviour of N=6 FAGNRs helixes.

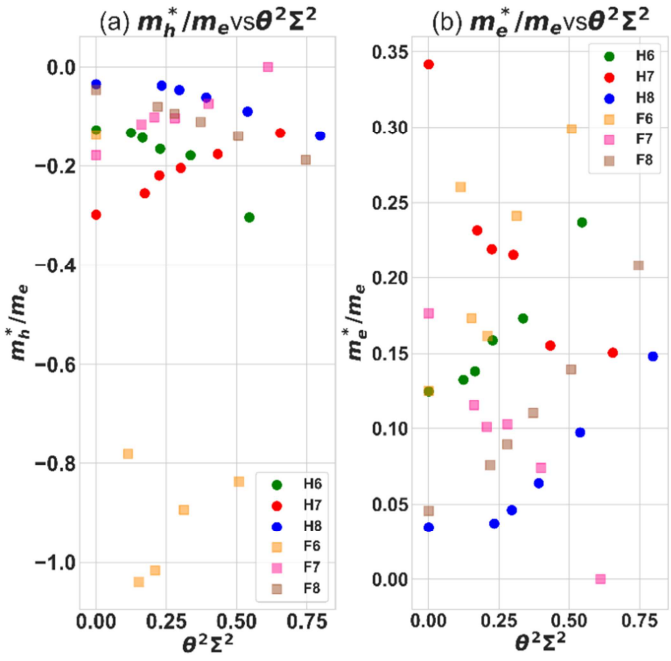

Figure 8: ***The response of (a) holes effective mass and (b) electron effective mass to effective torsional strain.***

The electrons (holes) mobilities for N=6, 7 and 8 untwisted FAGNRs are 9.5×10^3 (4.17×10^2), 2.98×10^2 (8.67×10^3) and 4.15×10^5 (1.82×10^3) $cm^2V^{-1}s^{-1}$, respectively. For N=6, 7 and 8 untwisted HAGNRs, the electrons (holes) mobilities are calculated to be 4.3×10^4 (2.92×10^2), 8.92×10^1 (2.0×10^3) and 2.42×10^3 (4.0×10^4) $cm^2V^{-1}s^{-1}$ respectively which are in good agreement with the electron mobilities of HAGNRs reported in ref [15]. Similar to the earlier reported results, it is found that the ideal N=3n wide HAGNR exhibits electrons' mobility comparable to the charge carriers' mobility of intrinsic graphene [15]. We also found that ideal N=3n+2 HAGNR holes' mobility is quite close to the charge carriers' mobility of intrinsic graphene. In the case of N=8 AGNRs the mobility of electron (hole) could be further increased (decreased) through F passivation up to 4.15×10^5 (1.82×10^3) $cm^2V^{-1}s^{-1}$. Thus, the control of the ribbon's width along with the passivation is crucial for determining the n-type or p-type of ribbons. Also, N=8 FAGNRs helixes have the best

electron carrier transmitting capacity and the biggest difference between the electron and hole mobility among all considered cases that suggest its n-type characteristic.

The electron (holes) carrier mobility of N=7 FAGNRs helixes is ~5 (~3) times larger than N=7HAGNRs' electron (holes) carrier mobility, whereas, the electron (holes) carrier mobility of N=6 H-AGNRs helixes is ~10 (~10) times larger than that of N=6 FAGNRs. Interestingly, for N=8 the electron (holes) carrier mobility of FAGNRs is of the order ~1/100 (~100) times smaller (larger) than electron (holes) carrier mobility of HAGNRs. As a function of twisting, the carrier mobilities decreased (Figure 9) for N= 6 and 8 FAGNRs and HAGNRs helixes. For example, in N=6 HAGNRs, electrons (holes) mobility decreases from $4.30x10^4$ ($2.92x10^2$) $cm^2V^{-1}s^{-1}$ to $1.65x10^4$ ($7.91x10^1$) $cm^2V^{-1}s^{-1}$ and for N=8 H-AGNRs it decreases from $2.42x10^3$ ($4.0x10^4$) $cm^2V^{-1}s^{-1}$ to $2.74x10^2$ ($5.04x10^3$) $cm^2V^{-1}s^{-1}$. However, in the case of N=7 HAGNRs the mobility gets increased from $8.92x10^1$ ($2.0x10^3$) $cm^2V^{-1}s^{-1}$ to $3.05x10^2$ ($6.70x10^3$) $cm^2V^{-1}s^{-1}$. The most twisted configuration of N=7 FAGNRs has the Dirac cone formation at the largest twist resulting in ballistic conductance and calculation of its mobilities goes beyond the scope of DP theory. It is clear from Figure 9 that electron (hole) mobility for N=8 FAGNRs is $4.15x10^5$ ($1.82x10^3$) $cm^2V^{-1}s^{-1}$ is comparable to graphene's charge carriers mobility. Also, it has the most sensitive and monotonous response to torsional strain. We find that the twisted AGNRs with appreciable bandgaps have relatively very high mobility (e.g. for HAGNRs~$4.30x10^4$ $cm^2V^{-1}s^{-1}$ and for FAGNRs ~$4.15x10^5$ $cm^2V^{-1}s^{-1}$), thus 'on-off' ratio may be way higher than TMDs (e.g. MoS_2 ~500 $cm^2V^{-1}s^{-1}$ [47]) and Black Phosphorene (~$2.6x10^4$ $cm^2V^{-1}s^{-1}$ [48,49]) monolayer.

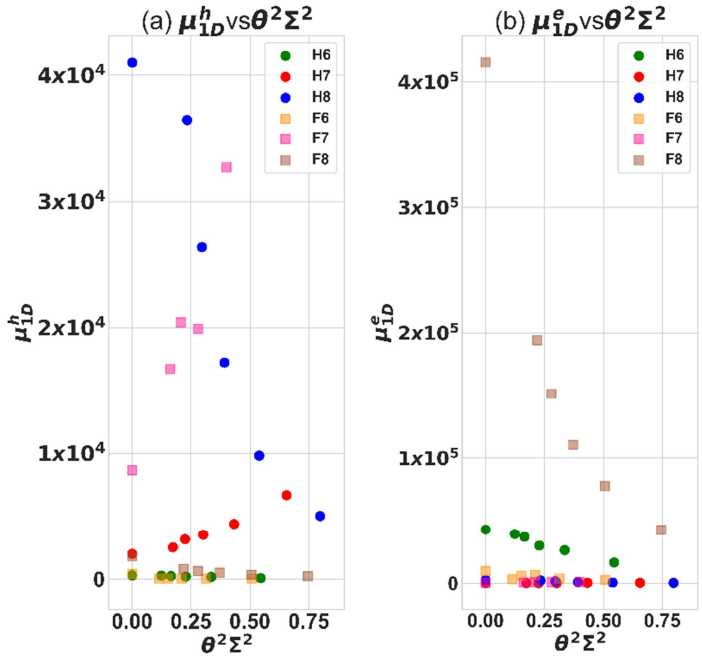

Figure 9: ***The response of (a) holes mobilities and (b) electron mobilities to effective torsional strain.***

4. Conclusion

In summary, we have calculated the electronic band structures and the intrinsic charge carrier mobilities of H and F passivated AGNRs as a function of torsional strains, using density functional theory combined with DP theory and effective mass approximation. From this study, following can be concluded:

(a) We find that the directness of the gap remains intact on twisting except in the case of N=6 F-AGNRs helixes. The bandgap varies monotonously as a function of torsional strain.

(b) The influence of twisted mode on electron-phonon or hole-phonon interaction is smaller than that of stretching mode; nonetheless, twisting has a profound effect on effective mass and mobility of AGNRs.

(c) The F passivation lowers the bandgap value of all N=7 HAGNRs topologies, however, it raises the bandgap value of all N=8 HAGNRs topologies. The longitudinal acoustic DP of hole (electron) is different for different AGNRs having an

order as $E_{1L}^{3n+2} > E_{1L}^{3n+1} > E_{1L}^{3n}$ ($E_{1L}^{3n} > E_{1L}^{3n+2} > E_{1L}^{3n+1}$) for H-AGNRs and as $E_{1L}^{3n+1} > E_{1L}^{3n} > E_{1L}^{3n+2}$ ($E_{1L}^{3n+2} > E_{1L}^{3n+1} > E_{1L}^{3n}$) for F-AGNRs.

(d) The electron (hole) carrier mobility of N=7 FAGNRs is ~5 (~3) times higher than N=7 HAGNRs, whereas, the electron (hole) carrier mobility of N=6 HAGNRs is ~10 (~10) times higher than N=6 FAGNRs. Interestingly, for N=8 the electron (holes) carriers mobility of FAGNRs are of the order of ~1/100 (~100) times smaller (higher) than its HAGNRs counterparts. The electron (hole) mobility has the following trend as $\mu_e^6 > \mu_e^8 > \mu_e^7$ ($\mu_h^8 > \mu_h^7 > \mu_h^6$) for HAGNRs and as $\mu_e^8 > \mu_e^6 > \mu_e^7$ ($\mu_h^7 > \mu_h^8 > \mu_h^6$) for FAGNRs. Due to the huge difference in hole and electron mobilities of N=8 and 6 FAGNRs, these emerge as n-type semiconductors.

Acknowledgments

High-performance computing facility of Centre for Development of Advanced Computing (CDAC), Pune and CVRAMAN, high performance computing cluster, at Himachal Pradesh University, Shimla has been used in obtaining the results presented in this paper which is gratefully acknowledged. Authors acknowledge the SIESTA team for providing code under a free license.

References

[1] Y.-C. Chen, T. Cao, C. Chen, Z. Pedramrazi, D. Haberer, D.G. de Oteyza, F.R. Fischer, S.G. Louie, M.F. Crommie, Molecular bandgap engineering of bottom-up synthesized graphene nanoribbon heterojunctions, Nat. Nanotechnol. 10 (2015) 156–160. https://doi.org/10.1038/nnano.2014.307.

[2] M. Kumar, N.K. Puri, N. Tyagi, P. Srivastava, Band Gap Engineering of Armchair Graphene Nanoribbons via Mn/Cr Termination, J. Comput. Theor. Nanosci. 14 (2017) 2401–2404. https://doi.org/10.1166/jctn.2017.6839.

[3] H.Y. He, Y. Zhang, B.C. Pan, Tuning electronic structure of graphene via tailoring structure: Theoretical study, J. Appl. Phys. 107 (2010) 114322. https://doi.org/10.1063/1.3437092.

[4] S. Fujii, T. Enoki, Cutting of Oxidized Graphene into Nanosized Pieces, J. Am. Chem. Soc. 132 (2010) 10034–10041. https://doi.org/10.1021/ja101265r.

[5] L. Tapasztó, G. Dobrik, P. Lambin, L.P. Biró, Tailoring the atomic structure of graphene nanoribbons by scanning tunnelling microscope lithography, Nat. Nanotechnol. 3 (2008) 397–401. https://doi.org/10.1038/nnano.2008.149.

[6] O.O. Kit, T. Tallinen, L. Mahadevan, J. Timonen, P. Koskinen, Twisting graphene nanoribbons into carbon nanotubes, Phys. Rev. B. 85 (2012) 085428. https://doi.org/10.1103/PhysRevB.85.085428.

[7] J. Jia, D. Shi, X. Feng, G. Chen, Electromechanical properties of armchair graphene nanoribbons under local torsion, Carbon N. Y. 76 (2014) 54–63. https://doi.org/10.1016/j.carbon.2014.04.048.

[8] P. Koskinen, Electromechanics of twisted graphene nanoribbons, Appl. Phys. Lett. 99 (2011) 013105. https://doi.org/10.1063/1.3607956.

[9] N. Al-Aqtash, H. Li, L. Wang, W.-N. Mei, R.F. Sabirianov, Electromechanical switching in graphene nanoribbons, Carbon N. Y. 51 (2013) 102–109. https://doi.org/10.1016/j.carbon.2012.08.018.

[10] M. Saiz-Bretín, F. Domínguez-Adame, A.V. Malyshev, Twisted graphene nanoribbons as nonlinear nanoelectronic devices, Carbon N. Y. 149 (2019) 587–593. https://doi.org/10.1016/j.carbon.2019.04.069.

[11] A.A. Fouladi, Effect of uniaxial strain on the tunnel magnetoresistance of T-shaped graphene nanoribbon based spin-valve, Superlattices Microstruct. 95 (2016) 108–114. https://doi.org/10.1016/j.spmi.2016.04.043.

[12] Z. Xie, T.Z. Markus, S.R. Cohen, Z. Vager, R. Gutierrez, R. Naaman, Spin Specific Electron Conduction through DNA Oligomers, Nano Lett. 11 (2011) 4652–4655. https://doi.org/10.1021/nl2021637.

[13] P. Xue, C. Chen, D. Diao, Ultra-sensitive flexible strain sensor based on graphene nanocrystallite carbon film with wrinkle structures, Carbon N. Y. 147 (2019) 227–235. https://doi.org/10.1016/j.carbon.2019.03.001.

[14] L. Zhang, X. Wang, Atomistic insights into the nanohelix of hydrogenated graphene: formation, characterization and application, Phys. Chem. Chem. Phys. 16 (2014) 2981. https://doi.org/10.1039/c3cp53978d.

[15] M. V Fischetti, J. Kim, S. Narayanan, Z.-Y. Ong, C. Sachs, D.K. Ferry, S.J. Aboud, Pseudopotential-based studies of electron transport in graphene and graphene nanoribbons, J. Phys. Condens. Matter. 25 (2013) 473202. https://doi.org/10.1088/0953-8984/25/47/473202.

[16] F. Ma, Z. Guo, K. Xu, P.K. Chu, First-principle study of energy band structure of armchair graphene nanoribbons, Solid State Commun. 152 (2012) 1089–1093. https://doi.org/10.1016/j.ssc.2012.04.058.

[17] T.W. Chamberlain, J. Biskupek, G.A. Rance, A. Chuvilin, T.J. Alexander, E. Bichoutskaia, U. Kaiser, A.N. Khlobystov, Size, Structure, and Helical Twist of Graphene Nanoribbons Controlled by Confinement in Carbon Nanotubes, ACS Nano. 6 (2012) 3943–3953. https://doi.org/10.1021/nn300137j.

[18] J. Park, W.C. Mitchel, S. Elhamri, L. Grazulis, J. Hoelscher, K. Mahalingam, C.

Hwang, S.-K. Mo, J. Lee, Observation of the intrinsic bandgap behaviour in as-grown epitaxial twisted graphene, Nat. Commun. 6 (2015) 5677. https://doi.org/10.1038/ncomms6677.

[19] Y. Lu, J. Guo, Band gap of strained graphene nanoribbons, Nano Res. 3 (2010) 189–199. https://doi.org/10.1007/s12274-010-1022-4.

[20] H. Suzuura, T. Ando, Phonons and electron-phonon scattering in carbon nanotubes, Phys. Rev. B. 65 (2002) 235412. https://doi.org/10.1103/PhysRevB.65.235412.

[21] D. Gunlycke, J. Li, J.W. Mintmire, C.T. White, Edges Bring New Dimension to Graphene Nanoribbons, Nano Lett. 10 (2010) 3638–3642. https://doi.org/10.1021/nl102034c.

[22] K. V Bets, B.I. Yakobson, Spontaneous twist and intrinsic instabilities of pristine graphene nanoribbons, Nano Res. 2 (2009) 161–166. https://doi.org/10.1007/s12274-009-9015-x.

[23] A. Shahabi, H. Wang, M. Upmanyu, Shaping van der Waals nanoribbons via torsional constraints: Scrolls, folds and supercoils, Sci. Rep. 4 (2015) 7004. https://doi.org/10.1038/srep07004.

[24] M. Topsakal, V.M.K. Bagci, S. Ciraci, Current-voltage (I-V) characteristics of armchair graphene nanoribbons under uniaxial strain, Phys. Rev. B. 81 (2010) 205437. https://doi.org/10.1103/PhysRevB.81.205437.

[25] I. Nikiforov, B. Hourahine, T. Frauenheim, T. Dumitrică, Formation of Helices in Graphene Nanoribbons under Torsion, J. Phys. Chem. Lett. 5 (2014) 4083–4087. https://doi.org/10.1021/jz501837r.

[26] C. Ma, Z. Xiao, A.A. Puretzky, A.P. Baddorf, W. Lu, K. Hong, J. Bernholc, A.-P. Li, Oxidization stability of atomically precise graphene nanoribbons, Phys. Rev. Mater. 2 (2018) 014006. https://doi.org/10.1103/PhysRevMaterials.2.014006.

[27] M. Liu, S. Chen, T. Li, J. Wang, D. Zhong, Tuning On-Surface Synthesis of Graphene Nanoribbons by Noncovalent Intermolecular Interactions, J. Phys. Chem. C. 122 (2018) 24415–24420. https://doi.org/10.1021/acs.jpcc.8b07618.

[28] J.M. Soler, E. Artacho, J.D. Gale, A. García, J. Junquera, P. Ordejón, D. Sánchez-Portal, The SIESTA method for ab initio order- N materials simulation, J. Phys. Condens. Matter. 14 (2002) 2745–2779. https://doi.org/10.1088/0953-8984/14/11/302.

[29] N. Troullier, J.L. Martins, Efficient pseudopotentials for plane-wave calculations, Phys. Rev. B. 43 (1991) 1993–2006. https://doi.org/10.1103/PhysRevB.43.1993.

[30] J.P. Perdew, K. Burke, M. Ernzerhof, Generalized Gradient Approximation Made Simple [Phys. Rev. Lett. 77, 3865 (1996)], Phys. Rev. Lett. 78 (1997) 1396–1396. https://doi.org/10.1103/PhysRevLett.78.1396.

[31] A. Kimouche, M.M. Ervasti, R. Drost, S. Halonen, A. Harju, P.M. Joensuu, J. Sainio, P. Liljeroth, Ultra-narrow metallic armchair graphene nanoribbons, Nat. Commun. 6 (2015) 10177. https://doi.org/10.1038/ncomms10177.

[32] P. Ruffieux, J. Cai, N.C. Plumb, L. Patthey, D. Prezzi, A. Ferretti, E. Molinari, X.

Feng, K. Müllen, C.A. Pignedoli, R. Fasel, Electronic Structure of Atomically Precise Graphene Nanoribbons, ACS Nano. 6 (2012) 6930–6935. https://doi.org/10.1021/nn3021376.

[33] H. Söde, L. Talirz, O. Gröning, C.A. Pignedoli, R. Berger, X. Feng, K. Müllen, R. Fasel, P. Ruffieux, Electronic band dispersion of graphene nanoribbons via Fourier-transformed scanning tunneling spectroscopy, Phys. Rev. B. 91 (2015) 045429. https://doi.org/10.1103/PhysRevB.91.045429.

[34] B. V Senkovskiy, D.Y. Usachov, A. V Fedorov, D. Haberer, N. Ehlen, F.R. Fischer, A. Grüneis, Finding the hidden valence band of N = 7 armchair graphene nanoribbons with angle-resolved photoemission spectroscopy, 2D Mater. 5 (2018) 035007. https://doi.org/10.1088/2053-1583/aabb70.

[35] L. Romaner, D. Nabok, P. Puschnig, E. Zojer, C. Ambrosch-Draxl, Theoretical study of PTCDA adsorbed on the coinage metal surfaces, Ag(111), Au(111) and Cu(111), New J. Phys. 11 (2009) 053010. https://doi.org/10.1088/1367-2630/11/5/053010.

[36] J. Cai, P. Ruffieux, R. Jaafar, M. Bieri, T. Braun, S. Blankenburg, M. Muoth, A.P. Seitsonen, M. Saleh, X. Feng, K. Müllen, R. Fasel, Atomically precise bottom-up fabrication of graphene nanoribbons, Nature. 466 (2010) 470–473. https://doi.org/10.1038/nature09211.

[37] X. Han, H.M. Stewart, S.A. Shevlin, C.R.A. Catlow, Z.X. Guo, Strain and Orientation Modulated Bandgaps and Effective Masses of Phosphorene Nanoribbons, Nano Lett. 14 (2014) 4607–4614. https://doi.org/10.1021/nl501658d.

[38] H.J. Monkhorst, J.D. Pack, Special points for Brillouin-zone integrations, Phys. Rev. B. 13 (1976) 5188–5192. https://doi.org/10.1103/PhysRevB.13.5188.

[39] R. Thakur, P.K. Ahluwalia, A. Kumar, M. Sharma, R. Sharma, Twisted Helical shaped Graphene Nano-Ribbons: Role of Symmetries and Passivation, Eprint ArXiv:1907.00567. (2019). http://arxiv.org/abs/1907.00567.

[40] D.-B. Zhang, T. Dumitrică, Role of effective tensile strain in electromechanical response of helical graphene nanoribbons with open and closed armchair edges, Phys. Rev. B. 85 (2012) 035445. https://doi.org/10.1103/PhysRevB.85.035445.

[41] F.L. Hirshfeld, Bonded-atom fragments for describing molecular charge densities, Theor. Chim. Acta. 44 (1977) 129–138. https://doi.org/10.1007/BF00549096.

[42] J. Bardeen, W. Shockley, Deformation Potentials and Mobilities in Non-Polar Crystals, Phys. Rev. 80 (1950) 72–80. https://doi.org/10.1103/PhysRev.80.72.

[43] Y.-W. Son, M.L. Cohen, S.G. Louie, Energy Gaps in Graphene Nanoribbons, Phys. Rev. Lett. 97 (2006) 216803. https://doi.org/10.1103/PhysRevLett.97.216803.

[44] J.-T. Sun, A.T.S. Wee, Y.P. Feng, Theoretical investigation of the electronic structures and carrier transport of hybrid graphene and boron nitride nanostructure, AIP Adv. 2 (2012) 032133. https://doi.org/10.1063/1.4745599.

[45] L. Yang, C.-H. Park, Y.-W. Son, M.L. Cohen, S.G. Louie, Quasiparticle Energies and Band Gaps in Graphene Nanoribbons, Phys. Rev. Lett. 99 (2007) 186801. https://doi.org/10.1103/PhysRevLett.99.186801.

[46] F.B. Beleznay, F. Bogár, J. Ladik, Charge carrier mobility in quasi-one-dimensional systems: Application to a guanine stack, J. Chem. Phys. 119 (2003) 5690–5695. https://doi.org/10.1063/1.1595634.

[47] R. Fivaz, E. Mooser, Mobility of Charge Carriers in Semiconducting Layer Structures, Phys. Rev. 163 (1967) 743–755. https://doi.org/10.1103/PhysRev.163.743.

[48] J. Xiao, M. Long, X. Zhang, J. Ouyang, H. Xu, Y. Gao, Theoretical predictions on the electronic structure and charge carrier mobility in 2D Phosphorus sheets, Sci. Rep. 5 (2015) 9961. https://doi.org/10.1038/srep09961.

[49] S. Kaur, A. Kumar, S. Srivastava, R. Pandey, K. Tankeshwar, Stability and carrier transport properties of phosphorene-based polymorphic nanoribbons, Nanotechnology. 29 (2018) 155701. https://doi.org/10.1088/1361-6528/aaac43.

Dear Editor,

The highlights of the study entitled as "*Electronic Structure and Carrier Mobilities of Twisted Graphene Helix*" are following.

(1) The band varies monotonously as a response to torsional strain. The influences of twisted modes electron-phonon or hole-phonon interaction is smaller than stretching modes, nonetheless, twisting has a profound effect on effective mass and mobilities.

(2) The longitudinal DP are different for hole and electron for different AGNRs having order for CBM (VBM) as $E_{1L}^{3n+2} > E_{1L}^{3n+1} > E_{1L}^{3n}$ ($E_{1L}^{3n} > E_{1L}^{3n+2} > E_{1L}^{3n}$) for HAGNRs and as $E_{1L}^{3n+1} > E_{1L}^{3n} > E_{1L}^{3n+2}$ ($E_{1L}^{3n+2} > E_{1L}^{3n+1} > E_{1L}^{3n+1}$) for FAGNRs.

(3) The numerical results indicate that the electrons (holes) mobilities of N=6 and 7 twisted FAGNRs at room temperature, are of the order ~0.1 (~0.1) times smaller and ~5 (~3) higher than its HAGNRs counterparts. Interestingly, for N=8 the electron (holes) carriers mobility of FAGNRs are of the order ~0.01 smaller (~100 higher) times than its HAGNRs counterparts.

(4) The trend of electron (holes) mobility as $\mu_e^6 > \mu_e^8 > \mu_e^7$ ($\mu_h^8 > \mu_h^7 > \mu_h^6$) for HAGNRs and as $\mu_e^8 > \mu_e^6 > \mu_e^7$ ($\mu_h^7 > \mu_h^8 > \mu_h^6$) for FAGNRs. Due to the huge difference mobilities in hole and electron, N=8 & 6 FAGNRs can be considered as n-type semiconductors.

Author Statement

Rajesh Thakur: Conceptualization, Software, Data Curation, Investigation, Writing - Original Draft. **P. K. Ahluwalia:** Writing - Review & Editing. **Ashok Kumar:** Writing - Review & Editing. **Brij Mohan:** Validation**. Raman Sharma:** Resources, Project administration.

Conflict of Interest and Authorship Conformation Form

Please check the following as appropriate:

- All authors have participated in (a) conception and design, or analysis and interpretation of the data; (b) drafting the article or revising it critically for important intellectual content; and (c) approval of the final version.
- This manuscript has not been submitted to, nor is under review at, another journal or other publishing venue.
- The authors have no affiliation with any organization with a direct or indirect financial interest in the subject matter discussed in the manuscript
- The following authors have affiliations with organizations with direct or indirect financial interest in the subject matter discussed in the manuscript:

Author's name	Affiliation
Rajesh Thakur	Himachal Pradesh University, Shimla, 171005, Himachal Pradesh (INDIA)
P. K. Ahluwalia	Himachal Pradesh University, Shimla, 171005, Himachal Pradesh (INDIA)
Ashok Kumar	*School of Basic and Applied Sciences, Central University of Punjab, Bathinda, 151001 Punjab (INDIA).*
Brij Mohan	*Department of Physics, Govt. Degree College Sanjauli, Shimla-171006, Himachal Pradesh (INDIA).*
Raman Sharma	Himachal Pradesh University, Shimla, 171005, Himachal Pradesh (INDIA)